Simulation of unsteady laminar flow in models of terminal aneurysm of the basilar artery

ALVARO VALENCIA*

Department of Mechanical Engineering, Universidad de Chile, Casilla 2777, Santiago, Chile

Blood flow dynamics play an important role in the pathogenesis and treatment of intracranial aneurysms. The evaluation of the velocity field in the aneurysm dome and neck is important for the correct placement of endovascular coils, in addition the temporal and spatial variations of wall shear stress in the aneurysm are correlated with its growth and rupture. The present numerical investigation describes the hemodynamics in two models of terminal aneurysm of the basilar artery. Aneurysm models with an aspect ratio of 1.0 and 1.67 were studied. Each model was subject to a steady, sinusoidal and physiologically representative waveform of inflow for a mean Reynolds number of 560. Symmetric and asymmetric outflow conditions in the branches were also studied.

The three-dimensional continuity and the Navier-Stokes equations for incompressible, unsteady laminar flow with Newtonian properties were solved with a commercial software using non structured grids with 61334 and 65961 cells for models 1 and 2, respectively. The grids were primarily composed of tetrahedral elements.

The intra-aneurysmal flow was unsteady for all input conditions and in both models, the flow always showed a complex vortex structure. The inflow and outflow zones in the aneurysm neck were determined. The wall shear stress on the aneurysm showed large temporal and spatial variations. The asymmetric outflow increased the wall shear stress in both models.

Keywords: Aneurysm; Basilar artery; CFD; Unsteady flow; Wall shear stress

1. Introduction

Blood flow in arteries is dominated by unsteady flow phenomena. The cardiovascular system is an internal flow loop with multiple branches in which a complex liquid circulates. The Womersley number characterizes the unsteady flow in the different arteries. The arteries are living organs that can adapt to and change with the varying hemodynamic conditions. In certain circumstances, unusual hemodynamic conditions create an abnormal biological response. Velocity profile skewing can create pockets in which the direction of the wall shear stress oscillates (Ku 1997). The relationship between flow in the arteries, particularly the wall shear stress, and the sites where diseases develop has motivated much of the research on arterial flow in recent decades (Berger and Jou 2000). It is now accepted that the sites where shear stresses are low or change rapidly in time or space are the ones that are most vulnerable (Lei *et al.* 1995). These conditions are likely to prevail at places where the vessel is curved; bifurcates; has a junction, a side branch, and when the flow is unsteady (Ku *et al.* 1985).

When an arterial wall loses its structural integrity, the result is the growth of a balloon-like bulge called a saccular aneurysm. The cerebral saccular aneurysm is a pathological dilation of an artery, generally found in and about the circle of Willis. Saccular aneurysms initiating at arterial bifurcations or along the cavernous segments of intracranial arteries may be of the lateral or terminal type. Saccular aneurysms display a variety of sizes and complex shapes. Most saccular aneurysms are located at the basilar bifurcation, middle cerebral, posterior communicating, anterior communicating, superior cerebellar, and posterior cerebral arteries (Parlea *et al.* 1999). Rupture of an intracranial saccular aneurysm generally causes subarachnoid hemorrhage (SAH), severe neurological complications and possibly death.

Hemodynamic factors, such as blood velocity, change the wall shear stress and the pressure. They play important roles in the pathogenesis of aneurysms and thromboses.

*Tel.: +56-2-6784386. Fax: +56-2-6988453. E-mail: alvalenc@ing.uchile.cl

Fluid flow in an aneurysm generally depends upon its geometric configuration and relation to the parent vessel, the size of the orifice and the volume of the aneurysm (Weir *et al.* 2003). Classical treatments of saccular aneurysms are direct surgical clipping or endovascular coil insertion. However, certain intracranial aneurysms are unamenable with these treatments because of their fusiform or complex wide-necked structure, giant size, or involvement with critical perforating of branch vessels. At present, proximal and distal occlusion (trapping) is the most effective treatment of these lesions. In lesions that cannot be trapped, alteration in blood flow to the inflow zone, which is the site that is most vulnerable to aneurysm growth and rupture, is used (Hoh *et al.* 2001). This strategy is based on the premise that aneurysm growth and rupture are functions of shear stress at the inflow zone. If the flow into the aneurysm can be altered in a way that the shear stress at the inflow zone is reduced, it is possible that the history of the lesion can be altered. For these reasons, hemodynamic studies on models of saccular aneurysms are very important in order to obtain quantitative criteria for appropriate treatment.

Liou and Liou (1999) presented a review of *in vitro* studies of hemodynamic characteristics in terminal and lateral aneurysm models. They reported in terminal aneurysms that for uneven branch flow, the flow activity inside the aneurysm and the shear stresses acting on the intra-aneurysmal wall increase with increasing bifurcation angle. There also exists a middle range of aneurysm size, above and below, which the forced vortex inside a terminal aneurysm is weaker, whereas in the middle range of aneurysmal size, the forced vortex is stronger and the fluctuation level is higher near the dome. In other words, the dome of a mid-size terminal aneurysm is subject to larger wall shear stress and vibrations. Ernemann *et al.* (2003) reported the influence of geometrical parameters on hemodynamics in *in vitro* models of aneurysms obtained with three-dimensional rotational angiography. Tateshima *et al.* (2001) studied the intra-aneurysmal flow dynamics in acrylic models obtained using three-dimensional computerized tomography angiography. They showed that the axial flow velocity structures were dynamically altered throughout the cardiac cycle, particularly at the aneurysm neck. Despite the fact that blood flow control is one of the key factors to improving the long-term anatomical outcome of aneurysm embolization, current diagnostic technologies do not have the capability to provide sufficient hemodynamic information. Therefore, the endovascular treatment of aneurysms may benefit from an accurate pretherapeutic evaluation of flow patterns in the aneurysm neck and dome using computational fluid dynamics (Tateshima *et al.* 2003). Although aneurysm rupture is thought to be associated with a significant change in aneurysm size, there is still great controversy regarding the size at which rupture occurs. Rupture occurs preferentially at the site of the dome, particularly in daughter aneurysms. The relationship between geometric features and rupture is closely associated with very low flow conditions (Ujiie *et al.* 1999).

Foutrakis *et al.* (1999) have presented the two-dimensional simulation of fluid flow in curved arteries and arterial bifurcations as well as the relationship between its hemodynamics and the formation and growth of aneurysms. The results suggest that the shear stress that develops along the outer wall of a curved artery and at the apex of an arterial bifurcation creates a hemodynamic state that promotes saccular aneurysm formation. Recently, Steinman *et al.* (2003) reported the image-based computational simulation of the flow dynamics for Newtonian fluid in a giant anatomically realistic human intracranial aneurysm with rigid walls. Computational fluid dynamics analysis revealed high-speed flow entering the aneurysm at the proximal and distal ends of the neck, promoting the formation of both persistent and transient vortices within the aneurysm sac. This produced dynamic patterns of elevated and oscillatory wall shear stresses distal to the neck and along the sidewalls of the aneurysm.

The influence of the non-Newtonian properties of blood on the flow in arteries was studied by Gijsen *et al.* (1999). They performed laser Doppler anemometry experiments and finite element simulations of steady flow in a three-dimensional model of the carotid bifurcation. A comparison between the experimental and numerical results showed good agreement, both for the Newtonian and the non-Newtonian fluid. Zhao *et al.* (2000) studied the flow in a model of a human carotid arterial bifurcation with rigid and compliant wall assumptions. Generally, there is a reduction in the magnitude of wall shear stress with compliant walls, its degree depending on the location and phase of the cardiac motion. However, the local differences are not large and the influence of compliant arterial walls can be considered as second-order effect compared to the influence of geometry and flow pulsatility.

Recently, Savaş (2002) performed flow visualization and particle imaging velocimetry in models of saccular basilar bifurcation aneurysms. Two flow models of varying spherical dome size were constructed out of clear silicone. Each model was subject to steady input flow conditions for a range of $Re = 175–650$. He also performed experiments with pulsatile input flow conditions at a mean $Re = 560$ with both sinusoidal and physiologically representative waveforms. Physiological and sinusoidal pulsatile input conditions with an asymmetric branching ratio caused the periodic appearance of a vortex-like circulation pattern in the dome of the smaller model. Planar instantaneous velocity field measurements showed highly three-dimensional flow patterns for the unsteady cases.

This paper presents detailed numerical simulations of the unsteady flow in two models of terminal saccular aneurysm of the basilar artery. The geometry and boundary conditions were adopted from the experimental work of Savaş. For both models, the effects of the branches' flow-rate ratio and inlet velocity profile on the

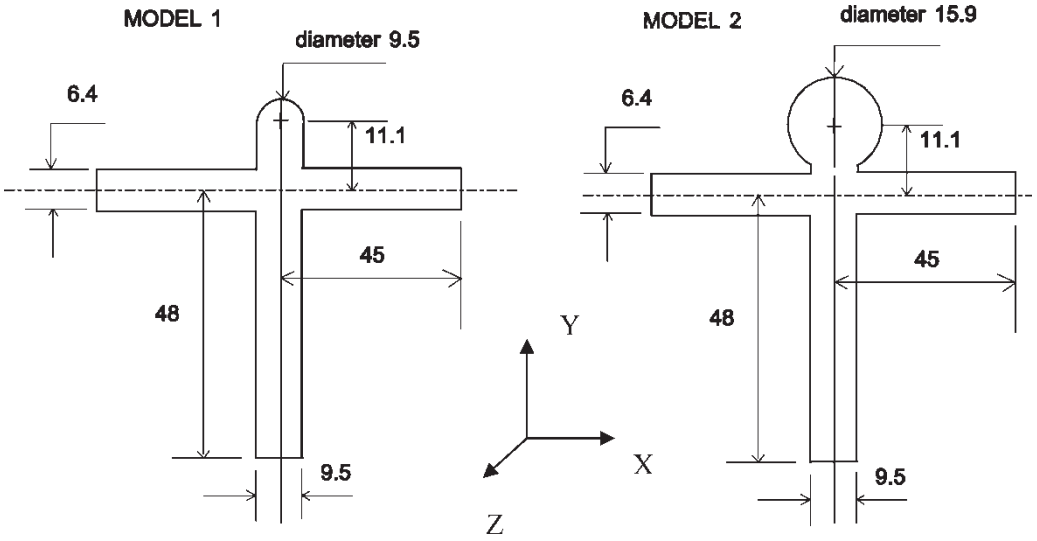

Figure 1. Flow model geometries, all dimensions are in [mm].

flow characteristics as well as on the shear stress on the aneurysmal wall are reported and discussed in this work.

2. Mathematical model and geometry

Basilar artery flow is assumed to be unsteady, three-dimensional and laminar. It is described by the continuity and Navier-Stokes equations for a Newtonian fluid. In this work, the effects of non-Newtonian fluid properties, wall elasticity, and anatomically realistic models have not been considered, as discussed in the section 1. The geometry of the two models of terminal aneurysm in the basilar artery is shown in figure 1. The bifurcation angle is 90°, with a symmetric placement of outflow tubes. Along with an aneurysm dome located symmetrically at the end of the input tube, the models form a perfect "T" shape. Physiologically, bifurcation geometry and aneurysm location show a great amount of irregularity and asymmetry. This work intends to mimic the flow conditions created by geometrical asymmetry by means of causing an asymmetric branching ratio of flow between the outflow tubes. Therefore, cases with both symmetric and asymmetric outflow were studied. For the cases with asymmetric outflow the branches flow-rate ratios were 0.65 and 0.35 of the inlet flow, respectively.

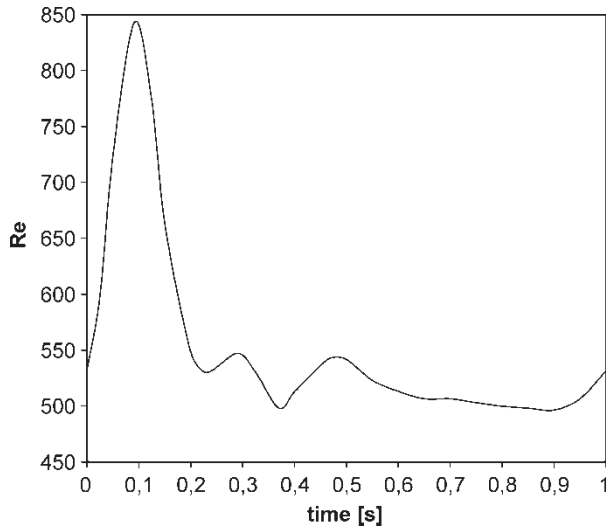

Figure 2. Physiological waveform, mean Reynolds number $Re = 560$.

The inlet velocity profile is assumed to be parabolic, given a mean flow velocity of $41.3\,\mathrm{cm\,s^{-1}}$, a basilar artery diameter of 0.475 cm, and the kinematic viscosity of blood at $0.035\,\mathrm{cm^2\,s^{-1}}$; the mean Reynolds number is 560. It should be noted that the numerical simulations were performed for the fluid used in the experimental work of Savaş (2002), with fluid kinematic viscosity at $0.14\,\mathrm{cm^2\,s^{-1}}$. In addition, the model has twice the diameter of a basilar artery, and therefore the input velocity needed to be doubled to $82.53\,\mathrm{cm\,s^{-1}}$, compared to physiological conditions. The application of pulsatile inflow also makes it necessary to match the Womersley number α with physiological conditions. It should further be noted that with the model diameter being twice as large as the physiological one and the working fluid four times as viscous as blood, it is unnecessary to change the pulse frequency, which is taken nominally here as 1 Hz.

The waveform shape was taken from an average waveform measured at the common carotid artery found in the literature, Berger and Jou (2000), and used by Savaş. Figure 2 shows the pulse with the fluid acceleration and deceleration phases during the systole and diastole phase respectively. The maximum and minimum Reynolds numbers are $Re_{\max} = 842$ and $Re_{\min} = 498$. The models are also exposed to a pulsatile inflow condition with a sinusoidal waveform for the same mean Reynolds number of 560. The peak-to-peak amplitude of the input waveform is matched to the physiological case, giving $Re_{\max} = 732$ and $Re_{\min} = 388$.

3. Numerical method

The governing equations were solved with the software Fluent, version 6.0 (Fluent, Inc., Lebanon, NH), which uses the finite volume method for the spatial discretization. The interpolations for velocities and pressure use power law and second order, respectively. The pressure–velocity coupling was obtained using the SIMPLEC algorithm. An explicit time-marching scheme with a small time step $\Delta t = 1 \times 10^{-4}$ s was used for the computed grid size. Fine unstructured grids with 61334 and 65961 cells were used for models 1 and 2, respectively. The unstructured grids were primarily composed of tetrahedral mesh elements, but included hexahedral, pyramidal and wedge elements where appropriate.

In order to check grid independence, numerical simulations of the flow in model 2 with steady inlet velocity and symmetric outflow were performed on grids with 46584, 65961 and 81746 cells. With the coarse grid the flow in the aneurysm was steady. Unsteady characteristics of the flow were only possible to be captured with the two finer meshes used. Differences in instantaneous local skin coefficients at several points of the aneurysm between the two finer grids were small. Therefore, the intermediate grid with 65961 cells with $\Delta t = 1 \times 10^{-4}$ s was used for the calculations of the unsteady flow in model 2.

The workstation used to perform the simulations in this work had a Pentium IV processor of 2.8 GHz clock speed, 512 MB RAM memory, and ran on a Linux Redhat v.8.0 operating system. The running time for a single simulation, based on 5 consecutive pulsatile flow cycles that use 5×10^4 iterations, was approximately 36 h of real time.

4. Results and discussion

Figure 3 shows intra-aneurysmal flow in the middle planes X–Y and Y–Z, see figure 1, with steady inflow and asymmetric outflow condition at $Re = 560$ for both models. The instantaneous velocity fields are shown for

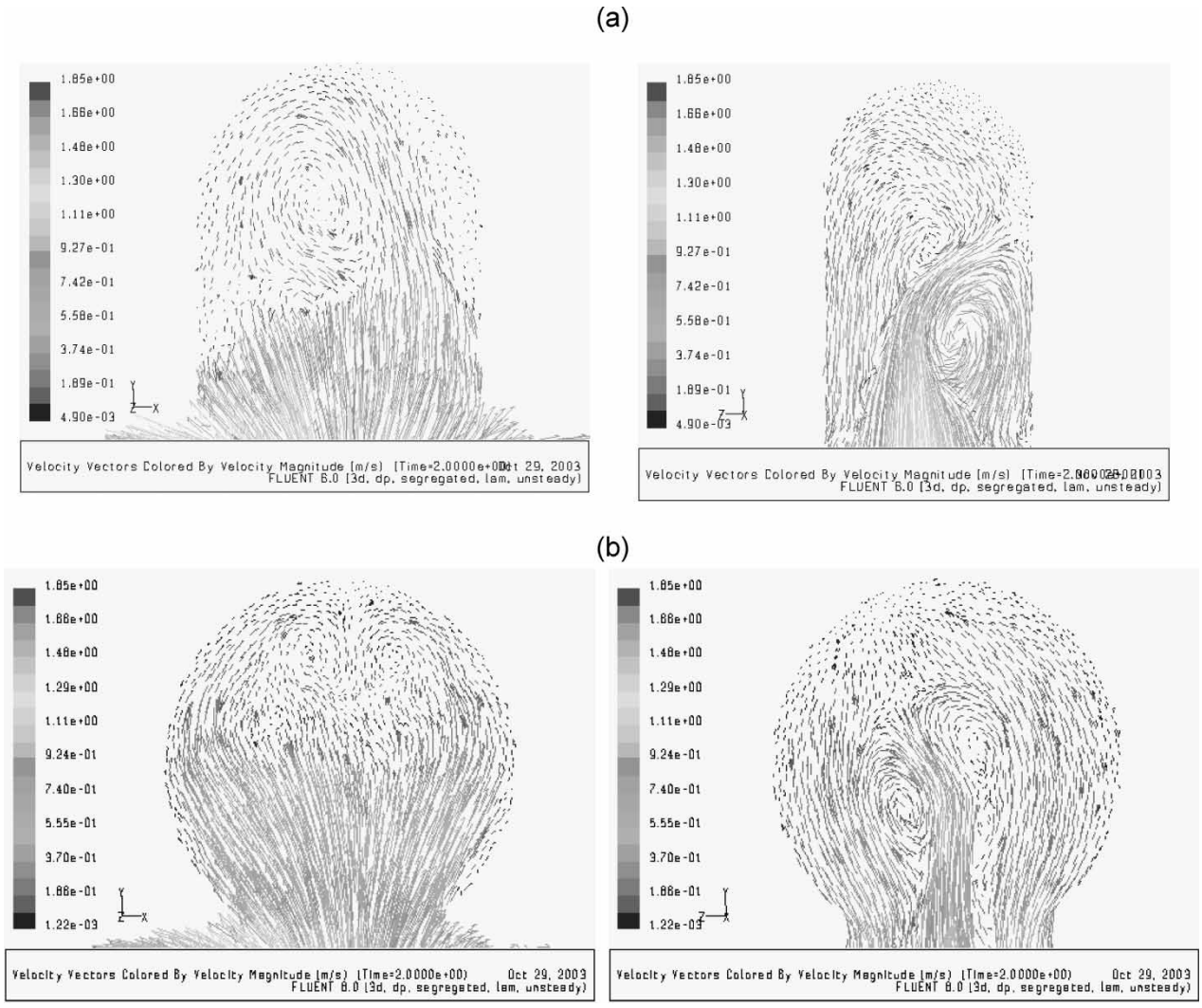

Figure 3. Velocity vectors at 2 s with steady inflow and asymmetric outflow. (a) Model 1, (b) model 2. Planes X–Y with $Z = 0$, and Y–Z with $X = 0$.

Table 1. Aneurysm flow oscillation frequency.

Case	f [Hz]
model 1 sy	10.8
model 1 asy	3.3
model 2 sy	10.2
model 2 asy	8.6

the computational time of 2 s. The intra-aneurysmal flow shows a complex vortex structure. The asymmetry of the outflow affects the intra-aneurysmal flow in both models, and the structure of the vortices in both models is asymmetric. The intra-aneurysmal velocities are lower in model 2 due to the spherical expansion of flow in this aneurysm.

The intra-aneurysmal flow is unsteady in both models for the cases with symmetric and asymmetric outflow conditions. Table 1 shows the frequency of flow oscillation in the aneurysm in both models with symmetric and asymmetric outflow conditions. The frequencies are larger than the normal physiological frequency in an artery, the self-sustained oscillating flow is only due to the aneurysm. This shows the potential of the aneurysm to disturb the flow around the bifurcation of the arteries.

Figure 4 shows the intra-aneurysmal flow in the middle planes $X-Y$ and $Y-Z$, with a physiologically representative waveform of inlet velocity and asymmetric outflow condition for the two models. The instantaneous velocity fields are shown for the computational time of 4.1 s. This time corresponds to the maximal inflow velocity or the end of the accelerating phase of the systole, see figure 2. The intra-aneurysmal flow shows similar vortex structure as with steady inlet velocity. The asymmetry of the outflow affects the intra-aneurysmal flow in both models, and again the structure of the vortices in both models is asymmetric.

The inflow and outflow zones in the aneurysm neck in both models can be observed in figure 4. The aneurysm neck did not show a simple flow pattern, as had previously been supposed in ideally shaped experimental *in vitro* aneurysms. The long-term anatomical durability of coil embolization of aneurysms by using existing microcoil

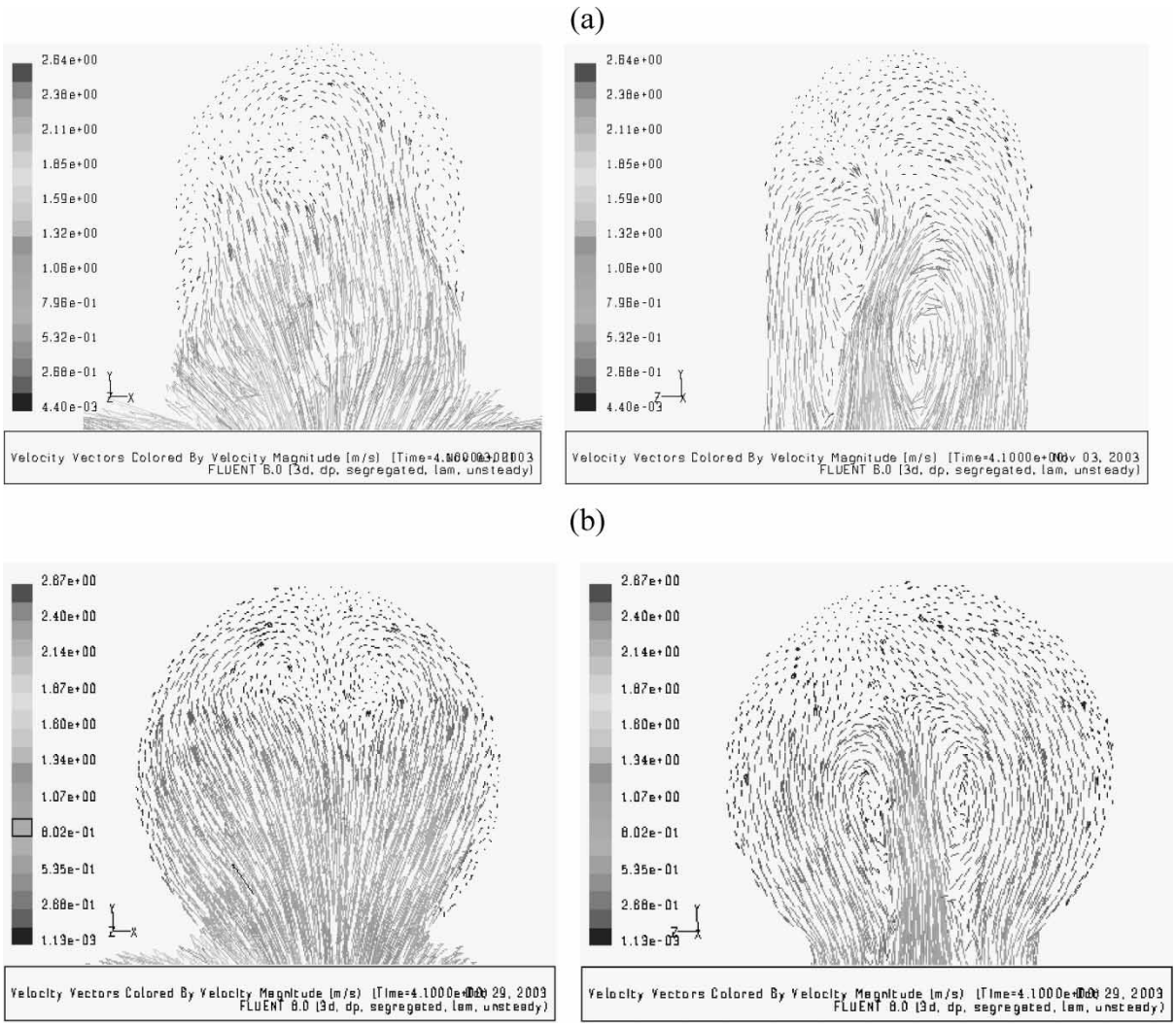

Figure 4. Velocity vectors at 4.1 s with physiologically representative waveform of inflow and asymmetric outflow. (a) model 1, and (b) model 2. Planes $X-Y$ with $Z = 0$, and $Y-Z$ with $X = 0$.

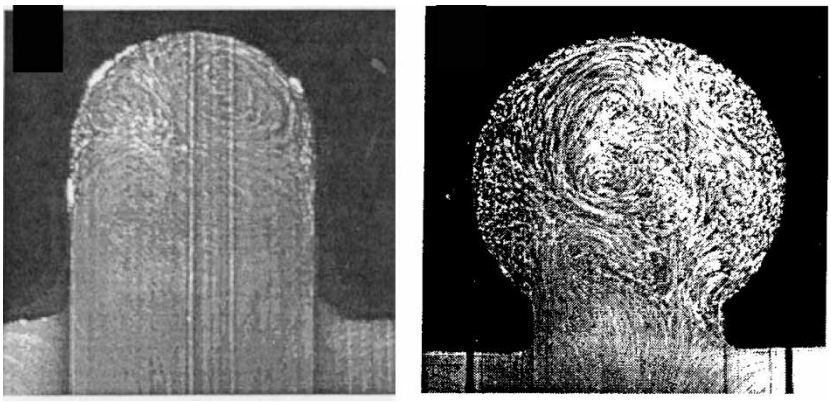

Figure 5. Experimental flow visualization of model 1 and 2 in plane $X-Y$ with $Z = 0$, $Re = 560$ (Savaş 2002).

technology depends on the aneurysm form and the blood flow dynamics in the aneurysm neck. Ideally the coil must be inserted into the inflow zone to avoid flow recanalization. The flow dynamics in the branches has secondary motion resulting from the turning of the stream as it enters the vessels, flow separation was observed in all cases at the inner side of the "T" as a result of the sharp turn the flow makes as it enters the junction.

Experimental flow visualization for models 1 and 2 on plane $X-Y$ with $Z = 0$ are shown in figure 5. The cases have a physiologically representative waveform of inflow and asymmetric outflow for $Re = 560$, Savaş (2002). At peak systole, the flow at the aneurysm top for model 1 displays significant unsteadiness and multiple vortices. In model 2, the flow unsteadiness reaches the aneurysm top and there is a large vortex generation beyond the neck. Comparison with the calculated velocity fields, figure 4 (a) and (b), shows differences in vortex structure. Probably, the reason for this is that the experimental flow becomes turbulent due to the vibration of the flexible model. As previously mentioned, the numerical results are valid for unsteady laminar flow only.

Figure 6 shows the time dependence of the skin friction coefficient at the aneurysm top, which is plotted over time for the cases with steady inflow in models 1 and 2. The wall shear stresses in model 1 are higher compared with those in model 2 for the same outflow condition. The asymmetry of the outflow increases the mean wall shear stress at a factor of 2.8 and 2.2 in models 1 and 2, respectively. The frequency of the wall shear stress in both models decreases with the asymmetry of outflow, see table 1.

The effects of the inlet velocity waveform on the skin friction coefficient at the aneurysm top over two time cycles is shown in figures 7 and 8 for models 1 and 2, respectively. The form of time dependence of the skin friction coefficient in the aneurysm is modulated with the inlet velocity waveform. With a physiologically representative waveform of inflow, the systolic acceleration phase and the diastolic deceleration phase produce both

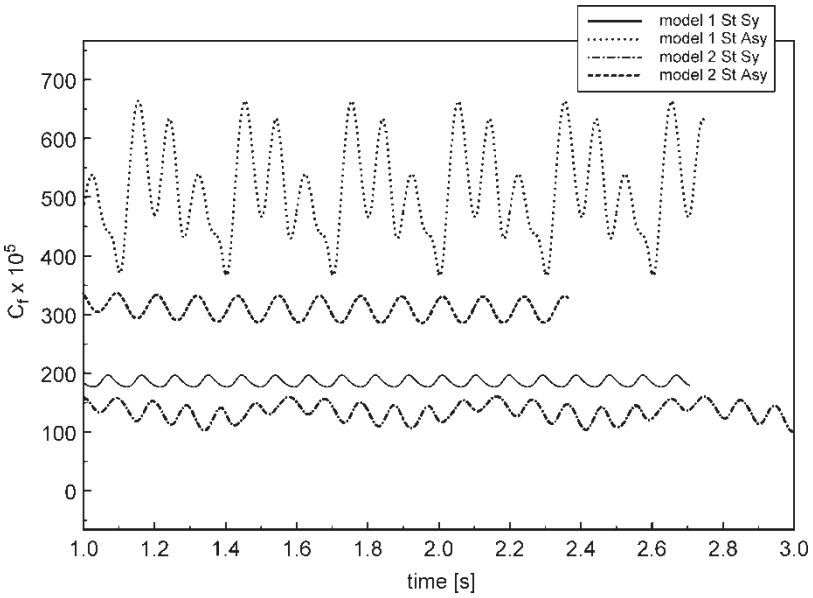

Figure 6. Skin friction coefficient at the aneurysm top plotted over time for the cases with steady inflow in model 1 and 2.

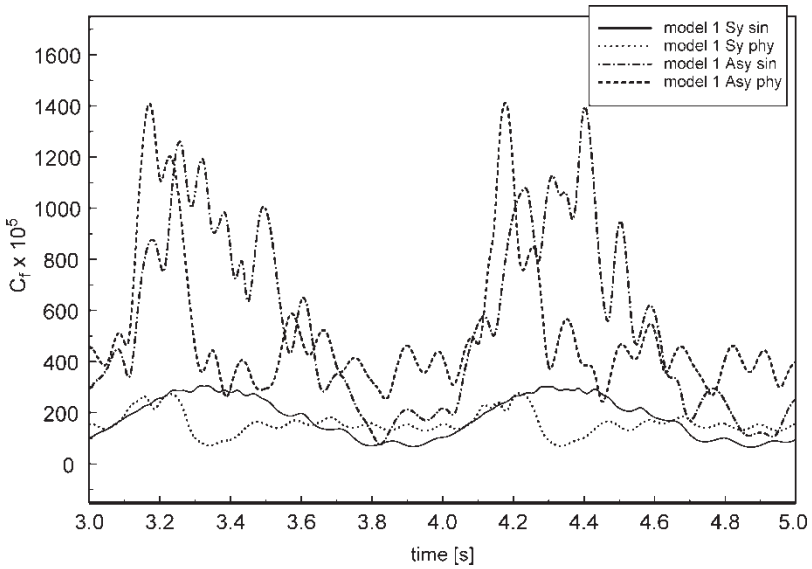

Figure 7. Skin friction coefficient at the aneurysm top plotted over time for model 1 for the cases with pulsatile inflow.

high and low velocity gradients on the aneurysm wall. With symmetric outflow, the values of wall shear stress in model 1 and 2 are similar. However, with asymmetric outflow, the mean values of wall shear stress in model 1 are larger at a factor of 1.6 than the mean values in model 2.

Savaş (2002) determined experimentally the wall shear stress at the aneurysm top in both models with a physiologically representative waveform of inlet velocity and asymmetric outflow. He reported maximum values of shear stresses in models 1 and 2 of 6 and 0.5 Pa, respectively. The numerically calculated maximum values of wall shear stresses in figures 7 and 8 for these cases reach 4 and 1.5 Pa, respectively. The numerical prediction of wall shear stress is not very close to the experimental result. This is a consequence of differences between numerically and experimentally determined velocity fields, as well as of the additional difficulty to experimentally measure time dependent wall shear stress from velocity fields of very low magnitude using PIV.

Figures 9 and 10 show time dependence of the skin friction coefficient in models 1 and 2 in five different points of plane $X-Y$ for $Z = 0$ on the aneurysm surface, for the cases with a physiologically representative waveform of inlet velocity and asymmetric outflow. The modulations of skin friction coefficients with the waveform of inlet velocity are clearly seen in figures 9 and 10. The values of the skin friction coefficient in the aneurysm neck in model 1 are larger than in model 2. The differences of the skin friction coefficient in points 1 and 5 are due to the asymmetric outflow.

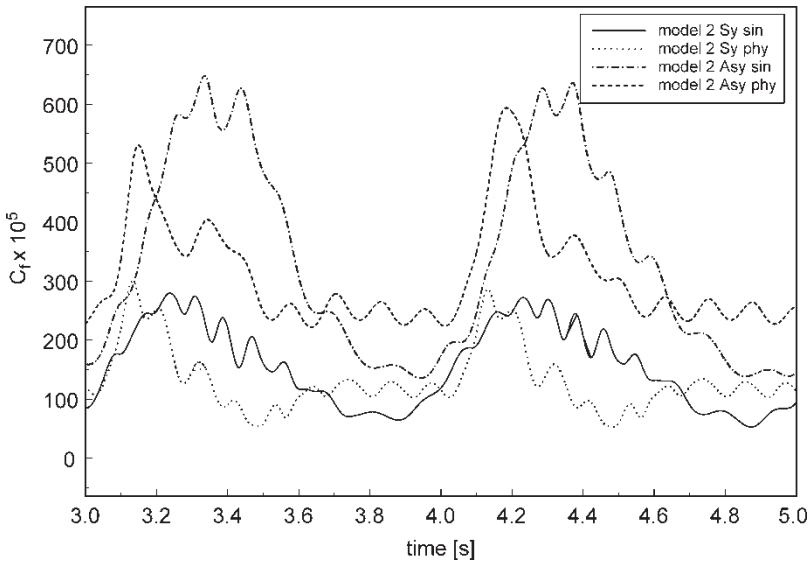

Figure 8. Skin friction coefficient at the aneurysm top plotted over time for model 2 for the cases with pulsatile inflow.

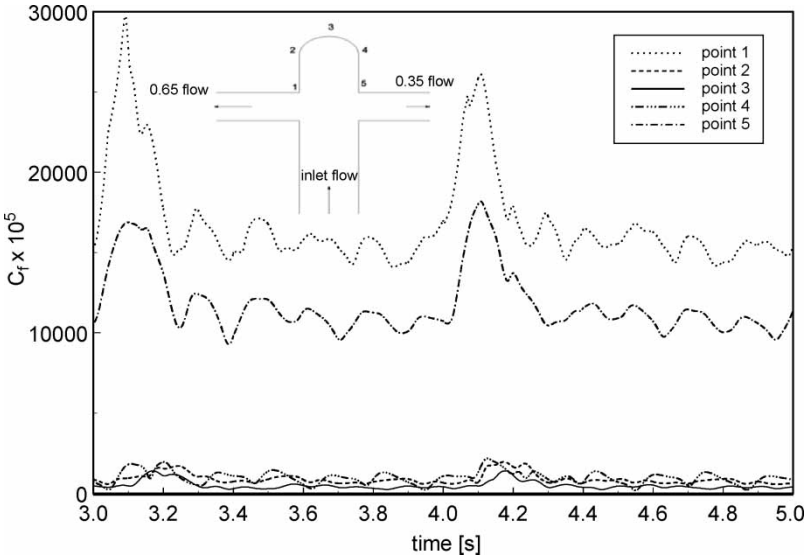

Figure 9. Variation of skin friction coefficient in the aneurysm of model 1 plotted over time in the plane $X-Y$ with $Z = 0$. Physiologically representative inlet velocity and asymmetric outflow.

Damage to the endothelium is seen as a contributing cause to aneurysm growth and rupture. Once the integrity of this layer of cells lining the lumen is breached, subsequent damage to the structural fibers of the vessel may occur. Blood flow is involved in the process leading to the damage of the endothelium. The correlation between fluctuating shear stresses and endothelial degeneration has been well documented in the literature. In this work, local shear stresses were found that showed considerable variation in time and position on the aneurysmal surface. This result suggests that damage occurs due to high amplitude shear stresses. This type of damage could include elements of fatigue as a consequence of the variations of wall shear stresses. In addition, the small flow velocities in the aneurysm can cause thrombosis.

This numerical study of hemodynamics provides insight into the vortex dynamics and wall shear stresses originated in hypothetical geometries of saccular aneurysms in the basilar artery. However, further investigations are required to consider the interaction of the compliant wall of the aneurysm, the transition to turbulence, and an anatomically realistic geometry.

5. Conclusions

The present numerical investigation describes the fluid flow in two models of terminal saccular aneurysm of the basilar artery. The effects of the aneurysm form and asymmetric outflow rates are studied in detail. The intra-aneurysmal flow in both models is unsteady for all studied

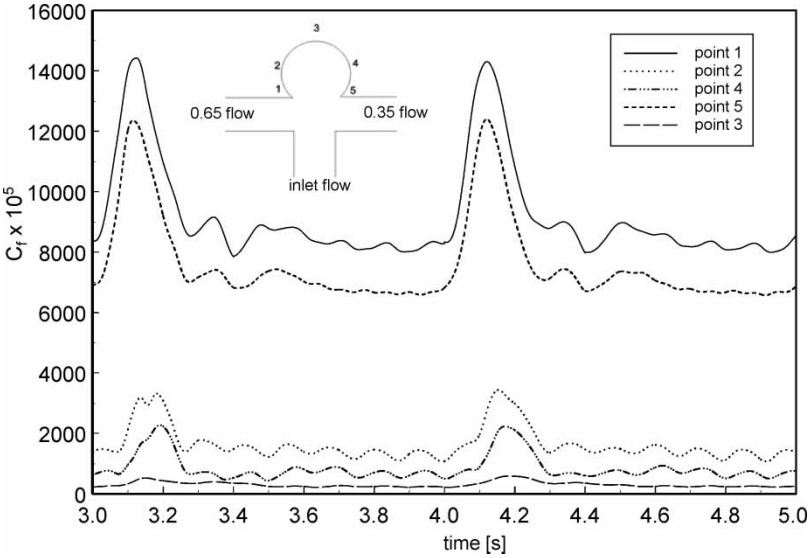

Figure 10. Variation of skin friction coefficient in the aneurysm of model 2 plotted over time in the plane $X-Y$ with $Z = 0$. Physiologically representative inlet velocity and asymmetric outflow.

inflow conditions. The flow shows an unsteady and complex vortex structure, and the flow in the aneurysmal neck has defined inflow and outflow zones. The comparison of velocity fields with available experimental flow visualizations shows differences in vortex structures. The influence of turbulence should be considered in the numerical simulation in order to obtain a better comparison with the experimental results.

Although the study of these two cases of terminal aneurysm with simplified geometry using computational fluid dynamics is not sufficient to reach any firm conclusions, the results obtained in these models indicate large spatial and temporal variation of shear stress on the aneurysm wall and the zones of inflow and outflow in the aneurysm neck. Further quantitative studies are necessary to investigate the effects of non-Newtonian fluid properties, wall elasticity, and of more realistic models on the development, growth, and rupture of intracranial aneurysms.

Nomenclature

C_f	skin friction coefficient $= \tau_W/(1/2\rho U_o^2)$
f	frequency [s^{-1}]
Re	Reynolds number $= U_o d/\nu$
U_o	mean velocity at inlet [$m\,s^{-1}$]
d	diameter [m]
p	pressure [Pa]
u	velocity [$m\,s^{-1}$]

Greek symbols

α	Womersley number $= (\omega d^2/\nu)^{0.5}$
μ	fluid viscosity [Pa s]
ν	fluid kinematic viscosity $= \mu/\rho$ [$m^2\,s^{-1}$]
ρ	density [$kg\,m^{-3}$]
ω	cardiac frequency [s^{-1}]

Acknowledgements

The financial support received from FONDECYT Chile under grant number 1030679 is recognized and appreciated. The author would also like to acknowledge and thank Professor Ö. Savaş, University of California at Berkeley, who has kindly provided experimental results.

References

Berger, S.A. and Jou, L.D., Flows in stenotic vessels. *Annu. Rev. Fluid Mech.*, 2000, **32**, 347–382.

Ernemann, U., Grönewäller, E., Duffner, F.B., Guervit, O., Claassen, J. and Skalej, M.D., Influence of geometric and hemodynamic parameters on aneurysm visualization during three-dimensional rotational angiography: An *in vitro* study. *AJNR Am. J. Neuroradiol.*, 2003, **24**, 597–603.

Foutrakis, G., Yonas, H. and Sclabassi, R., Saccular aneurysm formation in curved and bifurcating arteries. *AJNR Am. J. Neuroradiol.*, 1999, **20**, 1309–1317.

Gijsen, F.J., van de Vosse, F.N. and Janssen, J.D., The influence of the non-Newtonian properties of blood on the flow in large arteries: Steady flow in a carotid bifurcation model. *J. Biomech.*, 1999, **32**, 601–608.

Hoh, B.L., Putman, C.M., Budzik, R.F., Carter, B.S. and Ogilvy, C.S., Combined surgical and endovascular techniques of flow alteration to treat fusiform and complex wide-necked intracranial aneurysms that are unsuitable for clipping or coil embolization. *J. Neurosurg.*, 2001, **95**, 24–35.

Ku, D.N., Giddens, D.P., Zarins, C.K. and Glagov, S., Pulsatile flow and atherosclerosis in the human carotid bifurcation. *Arteriosclerosis*, 1985, **3**, 293–302.

Ku, D.N., Blood flow in arteries. *Annu. Rev. Fluid Mech.*, 1997, **29**, 399–434.

Lei, M., Kleinstreuer, C. and Truskey, G.A., Numerical investigation and prediction of atherogenic sites in branching arteries. *J. Biomech. Eng.*, 1995, **117**, 350–357.

Liou, T.M. and Liou, S.N., A review on *in vitro* studies of hemodynamic characteristics in terminal and lateral aneurysm models. *Proc. Natl Sci. Counc. Repub. China B*, 1999, **23**, 133–148.

Parlea, L., Fahrig, R., Holdsworth, D.W. and Lownie, S.P., An analysis of the geometry of saccular intracranial aneurysms. *AJNR Am. J. Neuroradiol.*, 1999, **20**, 1079–1089.

Savaş, Ö., Flow Visualization and Digital Particle Image Velocimetry on Model Bifurcation Aneurysms, 2002 (Department of Mechanical Engineering, University of California: Berkeley), Internal Document.

Steinman, D.A., Milner, J.S., Norley, C.J., Lownie, S.P. and Holdsworth, D.W., Image-based computational simulation of flow dynamics in a giant intracranial aneurysm. *Am. J. Neuroradiol.*, 2003, **24**, 559–566.

Tateshima, S., Murayama, Y., Villablanca, J.P., Morino, T., Takahashi, H., Yamauchi, T., Tanishita, K. and Viñuela, F., Intraaneurysmal flow dynamics study featuring an acrylic aneurysm model manufactured using a computerized tomography angiogram as a mold. *J. Neurosurg.*, 2001, **95**, 1020–1027.

Tateshima, S., Viñuela, F., Villablanca, J.P., Murayama, Y., Morino, T., Nomura, K. and Tanishita, K., Three-dimensional blood flow analysis in a wide-necked internal carotid artery-ophthalmic artery aneurysm. *J. Neurosurg.*, 2003, **99**, 526–533.

Ujiie, H., Tachibana, H., Hiramatsu, O., Hazel, A.L., Matsumoto, T., Ogasawara, Y., Nakajima, H., Hori, T., Takakura, K. and Kajiya, F., Effects of size and shape (aspect ratio) on the hemodynamics of saccular aneurysms: A possible index for surgical treatment of intracranial aneurysms. *Neurosurgery*, 1999, **45**, 119–130.

Weir, B., Amidei, C., Kongable, G., Findlay, J.M., Kassell, N.F., Kelly, J., Dai, L. and Karrison, T.G., The aspect ratio (dome/neck) of ruptured and unruptured aneurysms. *J. Neurosurg.*, 2003, **99**, 447–451.

Zhao, S.Z., Xu, X.Y., Hughes, A.D., Thom, S.A., Stanton, A.V., Ariff, B. and Long, Q., Blood flow and vessel mechanics in a physiologically realistic model of a human carotid arterial bifurcation. *J. Biomech.*, 2000, **33**, 975–984.